REPORT DOCUMENTATION PAGE

Form Approved OMB NO. 0704-0188

The public reporting burden for this collection of information is estimated to average 1 hour per response, including the time for reviewing instructions, searching existing data sources, gathering and maintaining the data needed, and completing and reviewing the collection of information. Send comments regarding this burden estimate or any other aspect of this collection of information, including suggesstions for reducing this burden, to Washington Headquarters Services, Directorate for Information Operations and Reports, 1215 Jefferson Davis Highway, Suite 1204, Arlington VA, 22202-4302. Respondents should be aware that notwithstanding any other provision of law, no person shall be subject to any oenalty for failing to comply with a collection of information if it does not display a currently valid OMB control number.
PLEASE DO NOT RETURN YOUR FORM TO THE ABOVE ADDRESS.

1. REPORT DATE (DD-MM-YYYY)	2. REPORT TYPE	3. DATES COVERED (From - To)
	New Reprint	-

4. TITLE AND SUBTITLE	5a. CONTRACT NUMBER
Material Modeling and Ballistic-Resistance Analysis of Armor-Grade Composites Reinforced with High-Performance Fibers	W911NF-09-1-0513
	5b. GRANT NUMBER
	5c. PROGRAM ELEMENT NUMBER
	622105

6. AUTHORS	5d. PROJECT NUMBER
M. Grujicic, P. S. Glomski, T. He, G. Arakere, W. C. Bell, B. A. Cheeseman	
	5e. TASK NUMBER
	5f. WORK UNIT NUMBER

7. PERFORMING ORGANIZATION NAMES AND ADDRESSES	8. PERFORMING ORGANIZATION REPORT NUMBER
Clemson University Office of Sponsored Programs 300 Brackett Hall Clemson, SC 29634 -5702	

9. SPONSORING/MONITORING AGENCY NAME(S) AND ADDRESS(ES)	10. SPONSOR/MONITOR'S ACRONYM(S)
U.S. Army Research Office P.O. Box 12211 Research Triangle Park, NC 27709-2211	ARO
	11. SPONSOR/MONITOR'S REPORT NUMBER(S)
	56526-EG.4

12. DISTRIBUTION AVAILIBILITY STATEMENT

Approved for public release; distribution is unlimited.

13. SUPPLEMENTARY NOTES

The views, opinions and/or findings contained in this report are those of the author(s) and should not contrued as an official Department of the Army position, policy or decision, unless so designated by other documentation.

14. ABSTRACT

A new ballistic material model for $0^\circ/90^\circ$ cross-plied oriented ultra-high molecular weight (UHMW) polyethylene fiber-based armor-grade composite laminates has been constructed using open-literature data for the fiber and polymeric-matrix material properties and the general experimental/field-test observations regarding the deformation and failure modes in these types of materials. The present model is an extension of our recently developed unit cell-based ballistic material model for the same class of composites (M. Grujicic, G. Arakere, T.

15. SUBJECT TERMS

armor-grade composites, failure analysis, high-performance fibers, material modeling, polymer-matrixcomposites

16. SECURITY CLASSIFICATION OF:			17. LIMITATION OF ABSTRACT	15. NUMBER OF PAGES	19a. NAME OF RESPONSIBLE PERSON
a. REPORT	b. ABSTRACT	c. THIS PAGE			Mica Grujicic
UU	UU	UU	UU		19b. TELEPHONE NUMBER
					864-656-5639

Standard Form 298 (Rev 8/98)
Prescribed by ANSI Std. Z39.18

Report Title

Material Modeling and Ballistic-Resistance Analysis of Armor-Grade Composites Reinforced with High-Performance Fibers

ABSTRACT

A new ballistic material model for $0\square/90\square$ cross-plied oriented ultra-high molecular weight (UHMW) polyethylene fiber-based armor-grade composite laminates has been constructed using open-literature data for the fiber and polymeric-matrix material properties and the general experimental/field-test observations regarding the deformation and failure modes in these types of materials. The present model is an extension of our recently developed unit cell-based ballistic material model for the same class of composites (M. Grujicic, G. Arakere, T. He,W.C. Bell, B. A. Cheeseman, C.-F. Yen, and B. Scott, A Ballistic Material Model for Cross-Plied Unidirectional Ultra-High Molecular-Weight Polyethylene Fiber-reinforced Armor-Grade Composites, Mater. Sci. Eng, A 2008, 498(1-2), p 231-241) which was found to be physically sound, but computationally not very efficient. The present model is constructed in such a way that it can be readily integrated into commercial finite element programs like ANSYS/Autodyn (ANSYS/Autodyn version 11.0, User Documentation, Century Dynamics Inc., a subsidiary of ANSYS Inc., 2007), as a User Material
Subroutine. To validate the model, a series of transient nonlinear dynamics computational analyses of the transverse impact of armor-grade composite laminates with two types of bullets/projectiles is carried out and the computational results compared with their experimental counterparts. Relatively good agreement is found between the experiment and the computational analysis relative to: (a) the success of the armor panels of different areal densities in defeating the bullets at different initial bullet velocities; (b) postmortem spatial distribution of the damage modes and the extents within the panels; (c) the temporal evolution of the armor-panel back-face bulge; and (d) The existence of three distinct armor-penetration stages (i.e., an initial filament shearing/cutting dominated stage, an intermediate stage characterized by pronounced filament/ matrix debonding/decohesion, and a final stage associated with the extensive filaments extension and armor panel back-face bulging).

REPORT DOCUMENTATION PAGE (SF298)
(Continuation Sheet)

Continuation for Block 13

ARO Report Number   56526.4-EG
Material Modeling and Ballistic-Resistance Analy   ...

Block 13: Supplementary Note
© 2009 . Published in Journal of Materials Engineering and Performance, Vol. Ed. 0 18, (9) (2009), (, (9). DoD Components
reserve a royalty-free, nonexclusive and irrevocable right to reproduce, publish, or otherwise use the work for Federal purposes,
and to authroize others to do so (DODGARS §32.36). The views, opinions and/or findings contained in this report are those of
the author(s) and should not be construed as an official Department of the Army position, policy or decision, unless so
designated by other documentation.

Approved for public release; distribution is unlimited.

Material Modeling and Ballistic-Resistance Analysis of Armor-Grade Composites Reinforced with High-Performance Fibers

M. Grujicic, P.S. Glomski, T. He, G. Arakere, W.C. Bell, and B.A. Cheeseman

A new ballistic material model for 0°/90° cross-plied oriented ultra-high molecular weight (UHMW) polyethylene fiber-based armor-grade composite laminates has been constructed using open-literature data for the fiber and polymeric-matrix material properties and the general experimental/field-test observations regarding the deformation and failure modes in these types of materials. The present model is an extension of our recently developed unit cell-based ballistic material model for the same class of composites (M. Grujicic, G. Arakere, T. He, W.C. Bell, B. A. Cheeseman, C.-F. Yen, and B. Scott, A Ballistic Material Model for Cross-Plied Unidirectional Ultra-High Molecular-Weight Polyethylene Fiber-reinforced Armor-Grade Composites, *Mater. Sci. Eng, A* 2008, 498(1-2), p 231-241) which was found to be physically sound, but computationally not very efficient. The present model is constructed in such a way that it can be readily integrated into commercial finite element programs like ANSYS/Autodyn (ANSYS/Autodyn version 11.0, User Documentation, Century Dynamics Inc., a subsidiary of ANSYS Inc., 2007), as a User Material Subroutine. To validate the model, a series of transient nonlinear dynamics computational analyses of the transverse impact of armor-grade composite laminates with two types of bullets/projectiles is carried out and the computational results compared with their experimental counterparts. Relatively good agreement is found between the experiment and the computational analysis relative to: (a) the success of the armor panels of different areal densities in defeating the bullets at different initial bullet velocities; (b) postmortem spatial distribution of the damage modes and the extents within the panels; (c) the temporal evolution of the armor-panel back-face bulge; and (d) The existence of three distinct armor-penetration stages (i.e., an initial filament shearing/cutting dominated stage, an intermediate stage characterized by pronounced filament/matrix debonding/decohesion, and a final stage associated with the extensive filaments extension and armor-panel back-face bulging).

1. Introduction

Fiber-reinforced polymer-matrix composites are among the most advanced commercially available materials nowadays. While they are widely used in aerospace and defense-related industries, their application in construction, automotive, and sporting-good industries is also quite common. The main reason for the aforementioned widespread use of the composite materials is their ability to simultaneously meet a variety of functional and manufacturing requirements. For example, the new Boeing 787 Dreamliner is primarily made of

M. Grujicic, P.S. Glomski, T. He, G. Arakere, and **W.C. Bell**, International Center for Automotive Research CU-ICAR, Department of Mechanical Engineering, Clemson University, Clemson, SC 29634; and **B.A. Cheeseman**, Army Research Laboratory – Survivability Materials Branch, Aberdeen Proving Ground, Aberdeen, MD 21005-5069. Contact e-mails: mica.grujicic@ces.clemson.edu, mica@ces.clemson.edu.

carbon-fiber-reinforced epoxy-matrix composites which, in addition to having outstanding mechanical properties, do not suffer from the similar manufacturing constraints as their metallic counterparts/alternatives, allowing a higher degree of optimization of the 787 aerodynamics. Furthermore, the composite airframes weigh less and are stronger than conventional airframes, which leads to improvements in the vehicle's operating efficiency and performance. Lastly, carbon-fiber-reinforced epoxy-matrix composites tend to resist corrosion and fatigue, the two phenomena which are well established to cause gradual degradation and ultimate failure of metallic airframes.

The fiber-reinforced polymer-matrix composites like the one described above in which the main figures of merit are their density-normalized stiffness (i.e., specific stiffness) and density-normalized strength (specific strength) are commonly referred to as "*structural-grade*" composites. Many blast- and ballistic-protection systems in military and civilian applications are, on the other hand, made of another class of fiber-reinforced polymer-matrix composites, the so-called "*armor-grade*" composites (Ref 1, 2). The latter class of composites generally is optimized with respect to its ballistic-impact protection resistance, i.e., with respect to its energy absorbing capability. Consequently, the most commonly cited figures of merit in these materials are: (a) a critical level of the projectile's velocity or the projectile's kinetic energy (generally referred to as the "*ballistic limit*") below which no full perforation of the armor

takes place (Ref 3, 4) and (b) an extent to which material ballistic-protection resistance is compromised in the armor systems which are partially penetrated by projectile(s) or whose strike-face surface is damaged by the projectile(s).

The armor-grade composites are generally constructed using high specific-modulus/high specific-strength polymeric fibers such as aramid (e.g., Kevlar®, Twaron®, etc.) or oriented polyethylene fibers (e.g., Spectra®, Dyneema®, etc.) with an outstanding impact resistance (Ref 5-9). The fibers, in the form of either woven fabrics or in the form of 0°/90° cross-plied collimated continuous filaments, are embedded in the resin/polymer matrix. To attain maximum utilization of the inherently high transverse-impact resistance of the fibers, the polymer-matrix content should not typically exceed 20% by volume. As a result of the very low resin content, these composites remain flexible/compliant to relatively high laminate thicknesses. Penetration resistance of the armor-grade composites is frequently increased through the use of hybrid structures in which a hard metallic or ceramic strike-plate is attached to the front of an armor-grade composite laminate.

Armor-grade composite laminates based on aramid fiber-reinforced phenolic-poly-vinyl-butyral resin and on 0°/90° cross-plied oriented polyethylene fiber-reinforced vinyl-ester resin are widely used in hard personnel-armor systems (e.g., protective helmets) for protection against fragments from exploding munitions (Ref 8-13). These armor-grade composites are also increasingly being used for ballistic protection in light-weight armored vehicles, helicopters, patrol boats, and transportable shelters (e.g., command shelters) (Ref 8). Furthermore, hybrid armor-grade composite structures with ceramic front strike-plates have been developed for bullet-protective armor systems.

Over the past decade, considerable efforts have been invested in carrying out various experimental investigations to identify and elucidate various penetration-failure mechanisms of the armor-grade fiber-reinforced composites under transverse impact loading and to compare and contrast these mechanisms with those operating in the related resin-free fabrics and resin-rich structural-grade composites. The main results obtained in these investigations can be summarized as follows (Ref 14-21):

(a) In sharp contrast to the penetration of resin-free fabrics which is dominated by the successive fracture of individual yarns along the periphery of the penetrator head and by the side-way/lateral movement of the yarns which enables them to slip off from the penetrator, the penetration of armor-grade composites is mainly governed by the failure of principal yarns (the yarns which are in direct contact with the penetrator head). This observation is attributed to the effect of resin matrix on reducing yarn mobility which prevents them from slipping off from the penetrator. In general, stiffer resin matrices (e.g., vinyl ester versus polyurethane) tend to constrain the yarn movement to a greater degree and to force the penetrator to engage and fracture more yarns during penetration. This typically results in improved ballistic-protection resistance of armor grade composites and is the reason that armor-grade composites reinforced with woven-yarn fabric are generally found to possess a higher energy-absorption potential than their resin-free fabric counterparts. However, excessive confinement of the yarns/filaments due to overly high matrix stiffness and/or excessive amounts of the matrix may have a deleterious effect on the ballistic-protection performance of this class of composites. The latter effect is related to the fact that highly confined fibers are more likely to fail in transverse shear before experiencing any significant extensions in the longitudinal direction;

(b) Since the energy absorbed by the armor-grade composite is found to scale with the number of broken yarns in its fabric constituent, fiber tensile straining and ultimate fracture is believed to be the dominant mechanism for absorption of the projectile kinetic energy;

(c) In addition to fiber fracture, both woven-fabric-reinforced and cross-plied fiber-reinforced composite laminates are generally found to include additional complex failure processes such as: (i) delamination, (ii) a plug punch-out, (iii) resin matrix cracking, and (iv) fiber pull-out. These failure modes are also typically observed in conventional structural-grade composites reinforced with glass or carbon fibers;

(d) In the case of multi-ply armor-grade composite laminates reinforced with either cross-plied collimated Spectra fibers or with woven Spectra fabrics, the following fracture modes are most often observed (Ref 22): (i) sequential delamination, (ii) plug punch-out induced by the through-the-thickness shear, and (iii) combined fiber shearing/cutting and fiber tensile failure. In the cross-plied laminates, fibers in the top plies are typically found to fail by shearing/cutting, primarily along the edges of the projectile. Fibers located in the back layers of the laminates, on the other hand, generally fail in tension; although in thin laminates, the lateral motion of fibers and/or fiber pull-out rather than fiber tensile-straining to fracture is sometimes observed;

(e) The delamination in the cross-plied Spectra fiber-reinforced composite laminates is typically found to resemble the "*generator strip*" phenomenon (Ref 20) seen in glass fiber-reinforced epoxy-matrix structural-grade composites. That is, under transverse impact, the projectile pushes a strip of the first lamina toward the rear of the laminate which induces shear cracks in the resin matrix parallel to the fibers and applies a transverse load to the second lamina. This, in turn, causes separation between the first two laminae, i.e., delamination. After the aforementioned delamination process had taken place successively through the entire thickness of the laminate via the same mechanism and penetration of the laminate has occurred, narrow strips of damage zone remain visible under transmitted light and the strips are found to tend to follow the respective fiber orientation in the panel. These strips typically contain numerous matrix/fiber interface cracks. In addition, a circular delamination zone is generally seen around the perforation hole;

(f) In contrast to the case of cross-plied fiber-reinforced composite laminates, fabric-reinforced laminates are found to exhibit much less lateral movements of reinforcing fibers during the penetration of the projectile (Ref 1, 2). Even in thin panels, fibers apparently failed due to shearing/cutting in the laminae near the strike-face and in tension at the rear of the completely penetrated laminates. The presence of a narrow strip of the first lamina pushed forward by the penetrator is generally not observed. Instead, the delamination zones are observed preferentially along the two reinforcement directions of woven fabric. However, these damage

zones are closely integrated with the circular delamination zone around the perforation hole. The occurrence of less anisotropic pattern of delamination was linked with the presence of resin-rich pockets between the reinforcing layers and with a greater constraint to matrix crack propagation parallel to the fibers/yarns; and

(g) Up to the thickness of ~3 mm, the kinetic energy for full perforation of armor-grade composites has been found to depend on the laminate thickness in a way similar to that observed in ductile monolithic materials (e.g., poly-carbonate or aluminum).

The full-perforation kinetic energy versus laminate thickness relationship, however, was found to be somewhat nonlinear. This finding has been attributed to the unique mode of tensile failure seen in these materials for which the critical level of kinetic energy for full perforation is lowered by the fiber/yarn mobility.

The first use of fiber-based composites (primarily nylon (*poly-amide*) fabric and *E-glass* fiber/ethyl cellulose composites) in body armor systems in place of the traditionally used metallic solutions can be traced back to the Korean War (Ref 23). Although, primarily due to their low cost, nylon and E-glass fibers are still being used today, high-performance polymeric fibers are now the standard in most fiber-reinforced body-armor applications. The high-performance polymeric fibers used today are characterized by substantially improved

strength, stiffness, and energy-absorbing capacity. Among these high-performance fibers, the most notable are: (a) *poly-aramids* (e.g., Kevlar®, Twaron®, Technora®); (b) highly oriented ultra-high molecular weight *poly-ethylene*, UHMWPE (e.g., Spectra®, Dyneema®); (c) *poly-benzobis-oxazole*, PBO (e.g., Zylon®), and (d) *poly-pyridobisimi-dazole*, PIPD (e.g., M5®). When tested in tension, all these materials differ significantly from the nylon fibers, having very high absolute stiffness, extremely high specific strength, and quite low ($<4\%$) strains-to-failure. These fibers essentially behave, in tension, as rate-independent linear elastic materials. When tested in transverse compression, however, these fibers are similar to nylon and can undergo large plastic deformation without a significant loss in their tensile load-carrying capacity. This behavior is quite different from that found in carbon or glass fibers, which tend to shatter under transverse compression loading conditions.

The ballistic performance of high-performance polymeric fibers is, in general, quantified with respect to their ability to: (a) absorb the projectile's kinetic energy locally and (b) spread out the absorbed energy fast before local conditions for the failure are met. In simple terms, the ability of high-performance fibers to absorb energy per their unit mass, E_{sp}, is related to the fiber tenacity/failure-strength, σ_{fail}, the fiber strain-to-failure, ε_{fail}, and the fiber density, ρ, as:

$$E_{sp} = 0.5\sigma_{fail}\varepsilon_{fail}/\rho \qquad (Eq\ 1)$$

The ability of fibers to spread out energy is governed by their speed of sound, v_{sound}, which is defined in terms of their axial modulus of elasticity, E, and their density as:

$$v_{sound} = (E/\rho)^{(1/2)} \qquad (Eq\ 2)$$

In Fig. 1, the two aforementioned ballistic performance parameters are displayed for the most-commonly used high-performance fibers. A summary of the key properties of the same set of high-performance fibers is provided in Table 1.

While the results displayed in Fig. 1 clearly reveal a high ballistic potential of the high-performance fibers in general (and specifically of the highly oriented UHMWPE fibers, the type of fiber-reinforcements considered in the present work), full utilization of this potential in armor-grade composites turned out to be a formidable challenge because a number of additional factors (e.g., fabric/ply structure/architecture, ply areal density, fiber-to-fiber/yarn-to-yarn and fiber/yarn-to-projectile friction, type of polymeric matrix, composite processing and fabrication conditions, shape, mass and mechanical properties of the projectile to be defeated, etc.) become important. To overcome these challenges, the development of flexible-armor systems has started to rely increasingly more on the use of transient nonlinear dynamics computational analyses of the ballistic response of armor
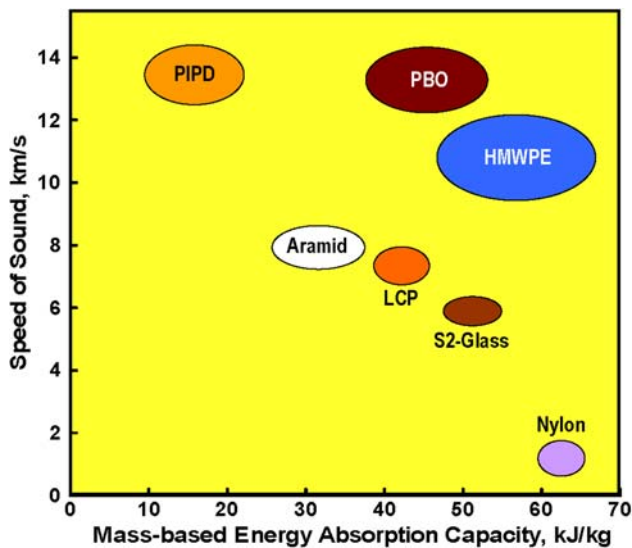

Fig. 1 Sound speed vs. mass-based energy absorption capacity for several high-performance fibers

Table 1 Typical mechanical properties of high-performance fibers

Fiber type	Failure strength, GPa	Failure strain	Axial modulus, GPa	Density, kg/m³
Aramid	2.8-3.2	0.015-0.045	60-115	1390-1440
HMWPE	2.8-4.0	0.029-0.038	90-140	970-980
LCP	2.7-2.9	0.033-0.035	64-66	1400-1420
PBO	5.4-5.6	0.024-0.026	270-290	1540-1560
PIPD	3.9-4.1	0.011-0.013	320-340	1690-1710
Nylon	0.06-0.08	1.5-2.5	1.0-1.5	1070-1170
S-glass	4.64-4.66	0.053-0.055	82-92	2470-2490

when impacted with high-speed projectiles. For these analyses to yield reliable predictions and for them to be used as complements to the accompanying experimental investigations, high-fidelity physically based material models for the armor-grade composite materials must be available.

A review of the public-domain literature carried out as part of the present work revealed the existence of several material models for armor-grade composites (Ref 24-29). While such models have provided an important insight into the roles of a number of factors mentioned above, they suffer from three major shortcomings: (a) They are more phenomenological, i.e., less physically based in their character; (b) They require the knowledge of a relatively large number of parameters; and (c) They are not very efficient computationally. These shortcomings seriously jeopardize the utility of the computational engineering analyses in the design and optimization of flexible armor systems for different projectile types and sizes. In addition to the models mentioned above, purely phenomenological models, e.g., Ref 30 also exist in the literature. Such models are the result of extensive experimental efforts and typically have, within the same family of armor-grade composite materials, a high practical utility. However, they provide no insight into the complicated physics of projectile/armor interactions and can not be used across the boundaries of different armor-type composite families.

To overcome the aforementioned limitations of the two groups of material models, a new physically based computationally efficient material model for UHMWPE-filament (e.g., Spectra®, Dyneema®, etc.) based armor-grade composites was recently developed by Grujicic et al. (Ref 22). Since it was found that for the UHMWPE fiber-based armor-grade composites, a substantially higher ballistic performance is obtained when such fibers are used as 0°/90° cross-plied unidirectional layers of filaments rather than woven fabrics, only the former composite-laminate architecture was analyzed in Ref 22. While the material model developed in Ref 22, reviewed in more details in next section, was found to be physically sound and to yield predictions regarding the ballistic-protection resistance of the armor-grade composite in question and its failure mechanisms which are fully consistent with their experimental counterparts, the unit cell nature of the model made it computationally not very efficient. In the present work, the material model for UHMWPE filament-based armor-grade composites of Grujicic et al. (Ref 22) has been further developed to address its computational efficiency. In passing, it should be mentioned that it is believed that the deflection of stress waves at the yarn/yarn or fiber/fiber cross-over points in woven fabric (the process which lowers the ability of fibers to spread out energy along their axis) is the main reason for their inferior ballistic performance.

The organization of the paper is as follows: A brief overview of a typical transient nonlinear dynamics computational procedure of the projectile/target interactions is given in section "Transient Nonlinear Dynamics Modeling of Projectile/Target Interactions". The procedure used to validate the material model for a prototypical 0°/90° cross-plied unidirectional UHMWPE filament-based armor-grade composite is discussed in section "Problem Description, Modeling, and Simulations". An overview of the armor-grade composite material model developed in Ref 22 and its further development are presented in section "Materials Modeling". Main results obtained in the current work are presented and discussed in section "Results and Discussion". The main summary points

and conclusions resulting from the present work are listed in section "Conclusions".

2. Computational Procedure

2.1 Transient Nonlinear Dynamics Modeling of Projectile/Target Interactions

The interactions between a projectile (full-metal jacketed armor-piercing and non-armor-piercing bullets, in the present work) and a target (0°/90° cross-plied oriented UHMWPE fiber-based armor-grade composite laminates, in the present work) have been carried out using ANSYS/Autodyn, a general-purpose transient nonlinear dynamics modeling and simulation software (Ref 31). Within ANSYS/Autodyn, the appropriate mass, momentum, and energy conservation equations are combined with the attendant-materials model equations and the appropriate initial and boundary conditions and solved numerically using a second-order accurate explicit scheme. The numerical framework (i.e., the "*processor*" as referred to in ANSYS/Autodyn) used is generally dependent on the physical nature of the problem being studied and, for multidomain problems, different domains can be analyzed using different processors. The Lagrange processor or the SPH (*Smooth Particle Hydrodynamics*) processor are typically used for solid-continuum structures, while the Euler processor is commonly used for modeling gases, liquids, or solids undergoing large deformations and density changes. The Lagrange-based Shell and Beam processors are designated for modeling shell- and beam-like solid structures, respectively.

In the present work, the ballistic-protection performance of 0°/90° cross-plied oriented UHMWPE fiber-based armor-grade composite laminates under single-hit bullet-impact threats was analyzed using the Lagrange processor. The interactions between the projectile and the target were accounted for through the use of the subdomain interaction options within ANSYS/Autodyn (Ref 31) which were overviewed in detail in our recent work (Ref 32). Also, a detailed discussion regarding the effect of the processor choice (Lagrange versus SPH) for the projectile and the target on the computational results can be found in Ref 32.

2.2 Problem Description, Modeling and Simulations

As stated earlier, the main objective of the present work was to develop a microstructure-dependent physically based computationally efficient material model for the armor-grade composites based on 0°/90° cross-plied unidirectional UHMWPE filaments and a low-content (<20 mass%) polymeric matrix. Details regarding the development of the material model are presented in section "Materials Modeling". In this section, a description is provided of the series of transient nonlinear dynamics analyses of the impact and penetration of armor-grade composite laminates by full-metal jacketed bullets which were carried out in the present work. A comparison of the obtained computational results with their experimental counterparts was next used in section "Results and Discussion" to conduct preliminary testing and validation of the material model developed in the present work.

Two types of full-metal jacketed bullets, both of the 5.56 mm caliber, were considered. The first type of bullet (M855) has a hardened steel tip attached to the lead core and a 0.5 mm thick copper jacket. The weight of this bullet is ~4.0 g and due to the presence of the hardened steel tip, the bullet

behaves as an armor-piercing projectile. The second bullet type (M193) does not contain a hardened steel tip but it is otherwise geometrically quite similar to the M855 bullet. The weight of the M193 bullet is ~3.5 g.

Since the computational results for the projectile/target impact obtained in the present work were compared with their experimental counterparts obtained in the work of Iremonger (Ref 33), five target panels with a thickness of 4.2, 11, 15, 22, and 32 mm were investigated in the present work. The corresponding target areal densities can be found in Table 2. In each case, the target panel had a circular disk shape with a radius of 90 mm.

Modeling and simulations were limited to the case of a normal impact of the composite laminate by the bullet and, due to the planar-isotropic nature of the problem, all the calculations are carried out using a three-dimensional (one-quarter) model while the appropriate symmetry boundary conditions are applied along the planes of symmetry. A simple schematic of the bullet/composite-laminate target impact/penetration problem analyzed here (and reflected across the two planes of symmetry) is depicted in Fig. 2.

Lagrange processors were used to represent both the bullet/ projectile and the target. Typically (one quarter of) the bullet was discretized in terms of ca. 2000 first-order tetrahedron elements, while (one quarter of) the composite-laminate target was discretized using ca. 400 first-order six-node brick elements, per 1.1 mm thick lamina. To reduce the computational burden, the size of the brick elements was chosen to match that of the tetrahedron elements only in the region of the composite-laminate target impacted and greatly affected by the bullet. A coarser mesh was used in the section of the panel less

affected by the bullet impact. An example of the initial meshes used in the bullet and the target panel is shown in Fig. 3.

The interactions between the projectile and the target were accounted for through the use of the subdomains interaction option within ANSYS/Autodyn (Ref 31) within which the contact-pressure/penetration relation is based on a penalty algorithm while the tangential interactions and sliding-friction resistance between the bullet and the target are accounted for using a simple Coulomb friction model.

Except for the symmetry surfaces, the projectile/target contact surfaces and lateral faces of the target, zero-stress boundary conditions are prescribed on all faces of the projectile and the target. To mimic the effect of clamping along the target edges, fixed boundary conditions were applied to all the peripheral nodes of the target panel.

To insure that the blast waves are not reflected at the lateral faces of the target, *transmit-type* boundary conditions were applied over the lateral target faces. The transmit-type boundary conditions enable propagation of the pressure waves across the boundaries without reflection mimicking wave propagation in an infinitely large domain (Ref 31). This type of boundary condition is typically used in problems which have only outward traveling solutions (e.g., an expanding high-pressure source). For such problems, to economize on problem size, it is advantageous to reduce the size of the computational domain. In practice, it proves impossible to include a simple boundary condition which is accurate for all wave strengths but the transmit condition implemented in ANSYS/Autodyn offers a reasonable approximation over a wide band. It should be noted, however, that the transmit boundary algorithm implemented in ANSYS/Autodyn pertains only to the normal component of velocity of the wave and the velocity component parallel to the boundary is assumed to be unaffected by the boundary.

Three metallic materials (steel, lead, and copper) are used to construct the two types of bullets while the target panel was made of the armor-grade composite material in question.

To define the initial conditions, zero initial velocities were assigned to all the nodes of the target panel while a constant velocity in the negative *z*-direction was assigned to all the nodes of the bullet. Four initial bullet velocities were considered: 600, 700, 800, and 900 m/s.

A standard mesh sensitivity analysis (the results not shown for brevity) was carried out to insure that the results obtained are effectively insensitive to the size of the cells or particles used.

Computational analyses were run on a machine with two 2.33 GHz Quad-core Intel Xeon processors with 16 GB of RAM. A typical run involving the 11 mm thick target panel took ~4 min while in the case of a 32 mm thick panel the

Table 2 Experimental (Ref 33) and the corresponding computational [Present Work] results pertaining to the success of armor-grade composite test panel to stop an M855 bullet at different initial bullet velocities

Test-panel thickness, mm	Areal density, kg/m²	Bullet velocity, m/s			
		600	700	800	900
4.2	4	...	...	...	G/G
11	10.5	G/G	G/G	G/G	G/G
15	13.7	...	O/O	O/O	G/G
22	21	U/U	U/U	U/U	U/U
32	31	U/U	U/U	U/U	U/U

U, Undermatched; O, Overmatched; G, Grossly overmatched; experiment/computation

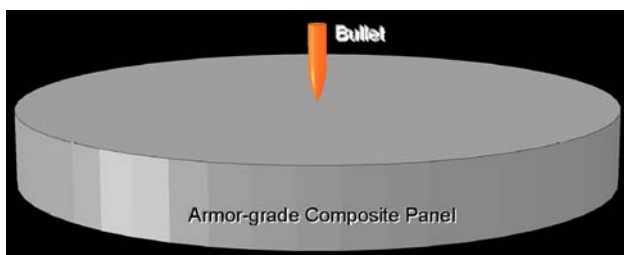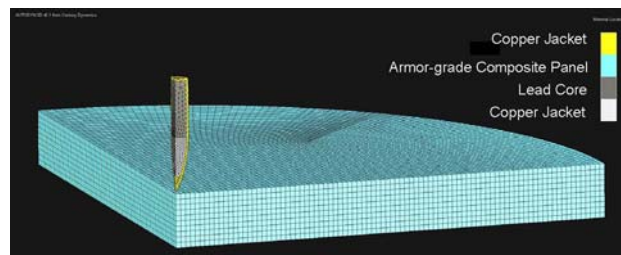**Fig. 2** A schematic representation of the normal impact of a bullet onto a circular disk-shaped armor-grade composite target

Fig. 3 An example of a typical finite element mesh of the bullet and armor-grade composite laminate used in the present work

wall-clock computational time was ~15 min. These times are about one-third of those encountered when the material model from Ref 22 was used while the level of experiment/computation agreement (discussed later) for the two material models was quite comparable.

2.3 Materials Modeling

As discussed in the previous section, to completely define a boundary value problem which will be analyzed using ANSYS/Autodyn, material-specific relations between the flow variables (pressure, stress, mass density, internal energy density, etc.) have to be specified. These relations typically involve: (a) an equation of state; (b) a strength equation; and (c) a failure equation for each constituent material. These equations arise from the fact that, in general, the total-stress tensor can be decomposed into a sum of a hydrostatic-stress (pressure) tensor (which gives rise to a change in the volume/density of the material) and a deviatoric-stress tensor (which is responsible for the shape change of the material). An equation of state is used to define mass-density (specific volume) and internal energy density (temperature) dependencies of the pressure. A strength model, on the other hand, combines yield criterion (the condition which must be met for plastic deformation to take place), a (plastic) flow rule (an equation defining relative magnitudes of the plastic-strain components), and a constitutive (strength) relation (an equation which defines the effect of plastic strain, the rate of deformation, and the temperature on material strength). Material degradation and failure are governed by a failure material model which describes the (hydrostatic or deviatoric) stress and/or strain conditions which, when met, cause the material to fracture and lose (abruptly, in the case of brittle materials or gradually, in the case of ductile materials) its ability to support tensile and shear stresses. Finally, when the Lagrange processor is used within ANSYS/Autodyn, an erosion material model can be used which enables the removal of highly distorted material elements/cells from the computational domain to prevent excessive numerical complications. When an element is eroded, its (freed) nodes are retained along with their velocities to conserve momentum of the system.

In the following, a brief description is given of the models for the materials utilized in the present work, i.e., for the metallic materials (steel, lead, and copper) present in the two types of bullets and armor-grade composites based on 0°/90° cross-plied unidirectional UHMWPE filaments and a low-content (<20 mass%) polymeric matrix. The values of the material model parameters for the metallic materials, defined in section "Metallic Materials", are available in the ANSYS/Autodyn materials library (Ref 31). The data cannot be disclosed here due to copyright violation concerns. The derivation and parameterization of the material model parameters for armor-grade composites based on 0°/90° cross-plied unidirectional UHMWPE filaments and a low-content (<20 mass%) polymeric matrix is presented in section "Computationally Efficient Armor-Grade Composites Material Model" in this paper and in Ref 22.

2.3.1 Metallic Materials. The three metallic materials (steel, lead, and copper) present in the two types of bullets were modeled using a linear equation of state, a von Mises yield criterion, the Prandtl-Reuss associative/normality flow rule, a Johnson-Cook strength model, a Johnson-Cook ductile-failure model, and an erosion model based on an instantaneous

geometrical strain of 2.0. Considering the fact that these material models were reviewed in our recent work (Ref 34), they will not be discussed any further here.

2.3.2 An Overview of Armor-Grade Composites Material Model (Ref 22). As stated earlier, the main objective of the present work is to improve computational efficiency of the material model for armor-grade composites based on 0°/90° cross-plied unidirectional UHMWPE filaments and a low-content (<20 mass%) polymeric matrix developed in Ref 22. As a first step toward meeting this objective, a brief overview of this model is provided in this section.

The material model developed in Ref 22 is of a unit cell type. The basic idea behind the unit cell-based approach is that the mechanical response of the armor unit cell (consisting of high-stiffness/high-strength polymeric filament segments and a compliant polymeric matrix) can be smeared out (homogenized) into an equivalent response of a (anisotropic) continuum material. A simple schematic of the unit cell which was used in Ref 22 to represent 0°/90° cross-plied unidirectional UHMWPE filament-based armor-grade composites allotted to a single-filament crossover is depicted in Fig. 4(a). Its continuum-level material point counterpart is represented in Fig. 4(b). Within the continuum material framework, filaments are not represented explicitly but rather by two material directions whose orientations are denoted in terms of material vectors, g_1 and g_2. The "*unit cell*" term is used to denote the basic structural block of an armor-grade composite material so that a panel made of this material can be viewed as a result of the repetition of this block in three orthogonal directions.
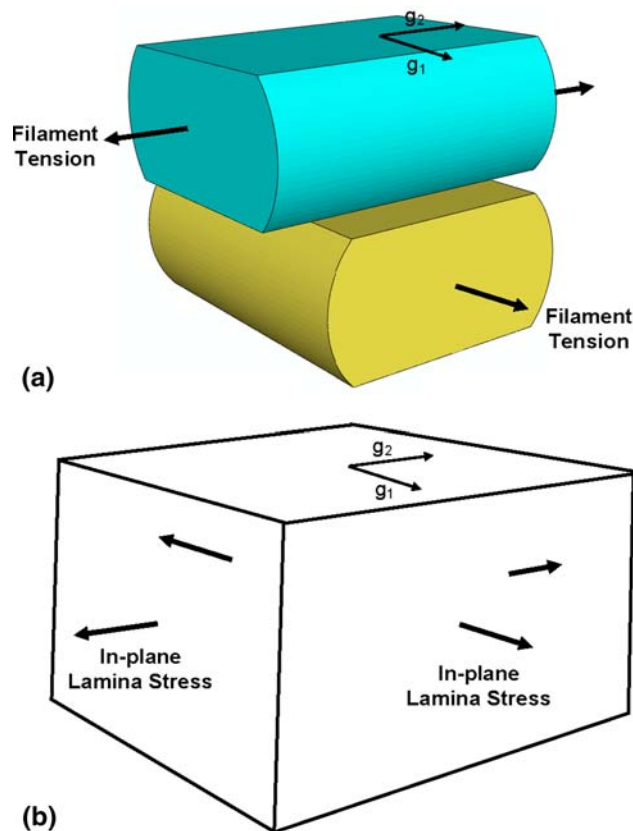

Fig. 4 The relationship between a unit cell and the corresponding material point in an anisotropic continuum (Ref 22)

Coupling between the continuum material formulation and the unit cell geometry and mechanical response was done in the following way: (a) the deformation state of a continuum material point (as quantified by the corresponding deformation gradient) is used to update the unit cell geometry; (b) the updated unit cell geometry and the state of the continuum material at the end of the previous time increment are used to update the extent of structural damage in the unit cell; and (c) the updated material state obtained in point (b) is then used to compute the stress state at the end of the current time increment.

The salient feature of the material model developed in Ref 22 was the assumption that the mechanical response of a continuum-level material point (corresponding to a unit cell in the armor-grade composite) and the accompanying changes in constituent materials (primarily those associated with the filament/matrix interfacial debonding) can be inferred by carrying out a series of finite element analyses pertaining to relatively simple mechanical tests of the unit cell. In these analyses, a detailed representation of the unit cell microstructure is considered.

In the aforementioned analyses, the polymeric filaments (assumed to be based on the UHMWPE) were modeled as orthotropic (more precisely as planar isotropic) linear elastic materials (up to the point of failure under axial tension or transverse shear), with the unique material direction being aligned with the filament axis. The polymeric matrix (assumed to be based on styrene-isoprene-styrene tri-block copolymer, Ref 32) was modeled, due to attendant high deformation rate conditions, as a linear isotropic material. Bonding between the filaments and the matrix was modeled using traction versus interfacial displacement discontinuity relations (one for the normal and one for the tangential displacements). These two relations were characterized by linear traction versus displacement-discontinuity relation unto the point of damage initiation and with a linear "*Down-Hill*" postdamage relationship. Consequently, the two modes (*normal* and *shear*) of interfacial-bonding damage were each characterized by three parameters: (a) critical normal or shear interfacial-displacement discontinuities at which damage initiation begins; (b) the corresponding normal or shear interfacial strengths; and (c) normal or shear interfacial-displacement discontinuities at which complete filament/matrix decohesion takes place. Interactions between the filaments and the matrix after decohesion were accounted for through a "*hard*" pressure versus over closure algorithm within which the interacting bodies must be in contact before they can interact and the pressure levels that can be transmitted through the contact interactions are unbounded. Relative sliding of the contacting bodies is opposed by a frictional force based on a constant friction coefficient.

The unit cell computational mechanical-testing analyses yielded the results which revealed that: (a) interfacial debonding was mainly caused by the through-the-thickness tension (in direction 3) and by the in-plane shear (1-2 shear); (b) E_{33}, G_{12}, G_{23}, and G_{31} normal and shear stiffness parameters were mostly degraded by interfacial debonding; and (c) these four stiffness parameters were found to degrade essentially linearly with the extent of interfacial-bonding damage, D. To account for these observations, a combined (through-the-thickness tension plus in-plane shear) quadratic interfacial debonding law was constructed.

Once the basic mechanical response of the unit cell to different loading modes was determined, homogenization of the unit cell into a continuum material point was carried out. The first step in this process was establishment of the relationship between the continuum-level material-point deformation state and the unit cell geometry. In general, six independent geometrical parameters are needed to fully describe the current geometry of the unit cell. These parameters include: (a) The three unit cell edge lengths, a_i (i = 1-3); (b) The in-plane shear interfilament included angle, θ; and (c) The two out-of-plane shear angles, ϕ and ψ. At the continuum level, the state of deformation at a given material point is described by the deformation gradient, F, whose components in a Cartesian coordinate system are defined as:

$$F_{jk}(t) = \frac{dx_j(t)}{dX_k} \qquad \text{(Eq 3)}$$

where $x_j(t)$ is the jth component of a material point at time t, and X_k the kth component of the same point in the initial/undeformed configuration.

At the continuum level, the 0° and 90° filaments can be described using vectors $\mathbf{a_i}$ (i = 1, 2) aligned with the axis of these filaments and the length of these vectors can be set equal to the corresponding current in-plane unit cell edge lengths, a_i (i = 1, 2). These vectors and the vector a_3 which is aligned with the out-of-plane unit cell edge can be related to their initial counterparts, $\mathbf{a_{i,0}}$ (i = 1-3) as:

$$\mathbf{a_i} = \mathbf{F a_{i,0}} \quad (i = \text{1-3}) \qquad \text{(Eq 4)}$$

The length of each $\mathbf{a_i}$ (i = 1-3) can be defined as:

$$a_i = \sqrt{\mathbf{a_i} \cdot \mathbf{a_i}} = \sqrt{(\mathbf{F a_{i,0}}) \cdot (\mathbf{F a_{i,0}})} = \sqrt{\mathbf{a_{i,0}}(\mathbf{F^T F}) \mathbf{a_{i,0}}} \qquad \text{(Eq 5)}$$

where the interfilament included angle θ can be computed from:

$$\mathbf{a_1} \cdot \mathbf{a_2} = (\mathbf{F a_{1,0}}) \cdot (\mathbf{F a_{2,0}}) = a_1 a_2 \cos\theta \qquad \text{(Eq 6)}$$

An equation analogous to Eq 6 can be used to define the out-of-plane shear angles ϕ and ψ. As shown in Ref 22, Eq 3-6 enable determination of the current geometry of the unit cell from the knowledge of the original unit cell edge lengths and the current value of the deformation gradient.

Once the current unit cell parameters are defined, standard relations were invoked in Ref 22 to compute the corresponding normal and shear strains. Next, through-the-thickness normal strain ε_{33} and the in-plane shear strain γ_{12} and the procedure outlined in the previous section were used to update the extent of material damage and the affected stiffness moduli. In this procedure, material damage was treated as irreversible, i.e., D was not allowed to decrease during the deformation history of a material point.

Next, the extent of material damage was updated. Then, E_{33}, G_{12}, G_{23}, and G_{31} stiffness coefficients were degraded by multiplying their initial values by a factor $(1.0 - cD)$, where $0.0 \leq c \leq 1.0$ is an elastic modulus-dependent parameter. Since the continuum material was modeled as a linear elastic orthotropic material with degradable stiffness moduli, the standard relationships are used to compute the stress components from the updated strain components and the updated material stiffness matrix.

Once the stresses were updated, the occurrence of filament failure was investigated. Filaments were allowed to fail in one of the two following modes: (a) in tension, when the tensile-strain/tensile-stress reaches a critical value or (b) due to

transverse shear, when the corresponding transverse shear stress reaches a critical value. When either of these two filament failure modes takes place, the corresponding in-plane normal stress(es) and the corresponding transverse shear stress were set to a small residual value associated with the remaining matrix ligaments. Once the stresses were updated to include the effect of filament failure, they were then returned to the finite element solver for the computation of the global equilibrium.

The material model developed in Ref 22 was, thus, constructed in such a way so that it can account for the competition between the following two processes: (a) Transverse-shear loading which is promoted by good filament/matrix bonding and higher matrix stiffness. If sufficiently high transverse shear stresses are developed, they can cause shear/type failure of the filament(s). In this case, the energy absorbed by the filaments is relatively small and, consequently, ballistic/protection performance of the armor-grade composite laminate is inferior and (b) Stretching of the filaments until the point of failure. This process is promoted by filament/matrix debonding which enables the filaments to deform independently of the matrix. In this case, the energy absorbed by the filaments is maximum and the ballistic/protection of the armor is greatly enhanced. It should be noted that some critical level of filament-matrix bonding is needed to insure that the filaments are not simply pushed laterally by the advancing projectile, which can lead to the defeat of the armor by the projectile via the so-called "*Wedge Through Effect*" (Ref 35).

Finally, the unit cell-based material model developed in Ref 22 was implemented in the material user subroutine, VUMAT, of the commercial finite element program ABAQUS/Explicit (Ref 36). This subroutine is compiled and linked with the finite element solver and enables ABAQUS/Explicit to obtain the needed information regarding the state of the material and the material mechanical response during each time step, for each integration point of each element.

2.3.3 Computationally Efficient Armor-Grade Composites Material Model. As mentioned earlier, the armor-grade composite material model developed in Ref 22 is physically very sound, but computationally not very efficient. While computational efficiency is generally not a critical point when analyzing single-hit projectile/test-panel interactions, it may become quite important when multi-hit projectile/real-target interactions or survivability of real targets (e.g., vehicles) to mine blast are analyzed. This is the reason that in this section an attempt is made to develop a more efficient material model for armor-grade composites. An example of a computationally efficient composite-material model can be found in Ref 37 in which E-glass-reinforced epoxy-matrix composite material was considered.

First, it should be noted that the 0°/90° cross-plied oriented UHMWPE fiber-based armor-grade composite material, considered here, is *in-plane* balanced and, hence, can be considered as being planar-isotropic. The $x_2 - x_3$ plane is chosen as the plane of isotropy and the through-the-thickness direction was taken to be parallel with the x_1-axis.

Equation of State. To comply with the E-glass/epoxy structural-composite material model (Ref 37), the equation of state is modeled as a sum of a polynomial volumetric part (accounts for linear and nonlinear contributions of mass density and internal energy density to pressure) and an orthotropic-elastic part (accounts for the contribution of the deviatoric strain components to pressure) as:

$$P = -K\mu + A_2\mu^2 - A_3\mu^3 + (B_0 - B_1\mu)\rho_0 e$$
$$- \frac{1}{3}(C_{11} + 2C_{12})e_{11}^d - \frac{1}{3}(C_{12} + C_{22} + C_{23})(e_{22}^d + e_{33}^d)$$

(Eq 7)

where P is pressure, K is the bulk modulus, $\mu = (\rho/\rho_0) - 1$ is the compression, ρ is the density, ρ_0 is the initial density, e is the mass-based internal energy density, C_{ij}s are the material stiffness coefficients (coefficients of the material 6×6 stiffness matrix), e_{ij}^ds are the components of the deviatoric strain matrix, and A_2, A_3, B_0, B_1 are material-specific parameters. It should be noted that the last term on the right-hand side of Eq 7 which represents the coupling between pressure and the deviatoric strain is absent in isotropic materials.

For a planar-isotropic material with an $x_2 - x_3$ plane of isotropy, the bulk modulus K is defined as:

$$K = \frac{1}{9}[C_{11} + 2C_{22} + 4C_{12} + 2C_{23}]$$ (Eq 8)

The elastic stiffness constants for the material at hand have been determined in Ref 22 using the aforementioned unit cell mechanical testing procedure. The results of this procedure are given in Table 3.

The mass-based internal energy density e is defined as:

$$e = C_v(T - T_{ref})$$ (Eq 9)

where C_v (=1850 J/kg·K, Ref 31) is the constant-volume specific heat, T is temperature, and T_{ref} (=298 K) is the corresponding zero-energy reference temperature.

Table 3 Orthotropic linear elastic material data for the 0°/90° cross-plied oriented UHMWPE fiber-based armor-grade composite material

E_{11}, GPa	E_{22}, GPa	E_{33}, GPa	G_{12}, GPa	G_{13}, GPa	G_{23}, GPa	v_{12}	v_{13}	v_{23}
93.0	93.0	11.5	4.6	5.0	5.0	0.0	0.1	0.5

C_{11}, GPa	C_{22}, GPa	C_{33}, GPa	C_{12}, GPa	C_{13}, GPa	C_{23}, GPa	C_{44}, GPa	C_{55}, GPa	C_{66}, GPa
96.4	95.9	12.2	6.5	6.4	5.9	9.2	10	10

S_{11}, GPa^{-1}	S_{22}, GPa^{-1}	S_{33}, GPa^{-1}	S_{12}, GPa^{-1}	S_{13}, GPa^{-1}	S_{23}, GPa^{-1}	S_{44}, GPa^{-1}	S_{55}, GPa^{-1}	S_{66}, GPa^{-1}
1.1×10^{-2}	1.1×10^{-2}	8.6×10^{-2}	-4.0×10^{-4}	-5.3×10^{-3}	-4.9×10^{-3}	1.1×10^{-1}	1.0×10^{-1}	1.0×10^{-1}

Strength Model. While the equation of state allows the computation of the pressure evolution during loading, the strength material model enables the entire stress tensor to be updated. During each computational time increment before failing, a material can undergo either elastic deformation or a combination of elastic and plastic deformations.

As stated earlier, to completely define a strength model, three relations must be defined: (a) a yield function and criterion, (b) a flow rule, and (c) a constitutive law.

A yield criterion is used to assess if the material's response is elastic or elastic/plastic. The yield criterion used in the present work is based on a total-stress six-parameter parabolic yield function in the form:

$$f(\sigma_{ij}) = a_{11}\sigma_{11}^2 + a_{22}\left(\sigma_{22}^2 + \sigma_{33}^2\right) + 2a_{12}\sigma_{11}(\sigma_{22} + \sigma_{33})$$
$$+ 2a_{23}\sigma_{22}\sigma_{33} + 2a_{44}\sigma_{23}^2 + 2a_{55}\left(\sigma_{31}^2 + \sigma_{12}^2\right) - R(\bar{e}^p)$$

(Eq 10)

where σ_{ij}s represent stress components, while a_{ij}s and R represent material specific parameters. It should be noted that one of the parameters in Eq 10 can be set independently. In the present work, a_{22} is set to 1.0 so that R is numerically equal to the square of in-plane yield (flow) strength of the composite material. As indicated in Eq 10, the parameter R can, for strain-hardening materials, increase with an increase in the magnitude of the equivalent plastic strain, $\bar{e}^p$.

The yield function coefficients a_{ij} appearing in Eq 10 are determined using the unit cell mechanical testing procedure described earlier. The onset of plasticity in each loading case was assumed to coincide with the condition when the equivalent plastic strain attains a value of 0.002. A summary of the results obtained in this portion of the work is given in Table 4.

To determine if the material's response will be elastic or elastic/plastic during a given time step, it is assumed that the material's response is purely elastic and the stress components are updated using the orthotropic linear-elastic stress-strain relationships. Updated stress components are then used in Eq 10 to compute the yield function, f. If $f < 0$, the material response is elastic and the updated stress components are retained and assembled to define the new stress state. Otherwise, the material response is elastic/plastic and the updated stress components define only an "*elastic predictor stress state*" which needs to be relaxed to the new material stress state by allowing plastic deformation to take place. A schematic of the Euler-backward computational procedure used to update the stress state during an elastic/plastic loading step is depicted in Fig. 5.

The second component of the strength model is a flow rule relationship which governs the direction of plastic flow during an elastic/plastic loading step. Following Ref 37, the Prandtl-Reuss associative plastic flow rule is used here which states that the material flows plastically in a direction which is co-linear with the stress-based gradient of the yield function (evaluated at the updated stress state). Since the Prandtl-Reuss associative flow rule is a universal relation, it does not require definition of any additional material parameters.

The third part of the strength model is the constitutive material law which describes strain-hardening effects on the intrinsic material ability to resist plastic deformation. Due to the fact that UHMWPE fibers (the dominant component in the armor-grade composite in question) are essentially linear elastic up to the point of failure, an ideal plastic constitutive material law is postulated. That is, the effects of strain hardening are assumed to be insignificant and, hence, could be neglected. Thus, the parameter R in Eq 10 can be set to a constant value equal to the square of the initial in-plane material yield strength (the latter quantity was obtained using the aforementioned unit cell mechanical-testing procedure).

Failure Model. Since the material at hand has limited ductility, upon exhausting its ability for further plastic deformation, it starts to fail. The failure takes place in a gradual manner, i.e., the material progressively loses its ability to support tensile normal and shear stresses. Once a material element begins to fail, the stress state in such element is subsequently updated using a failure model rather than a strength model. However, the orthotropic damage-induced softening/failure model, used in the present work, has a lot of mathematical similarities to the strength model discussed in the previous section. That is the orthotropic-softening failure model includes: (a) a failure initiation criterion; (b) a (damage) flow rule; and (c) a material degradation constitutive relation. It should be noted that, while in the case of the strength model the extent of inelastic deformation is quantified by the plastic strain components, in the case of failure the inelastic material response is quantified using the so-called "*crack-strain*" components.

Twelve material-specific parameters (six failure initiation strengths and six corresponding fracture energies) are used to define the failure model at hand. The six strength/fracture-energy components are associated with the six basic failure modes, i.e., the 11, 22, and 33 tensile-failure modes, and the 23,
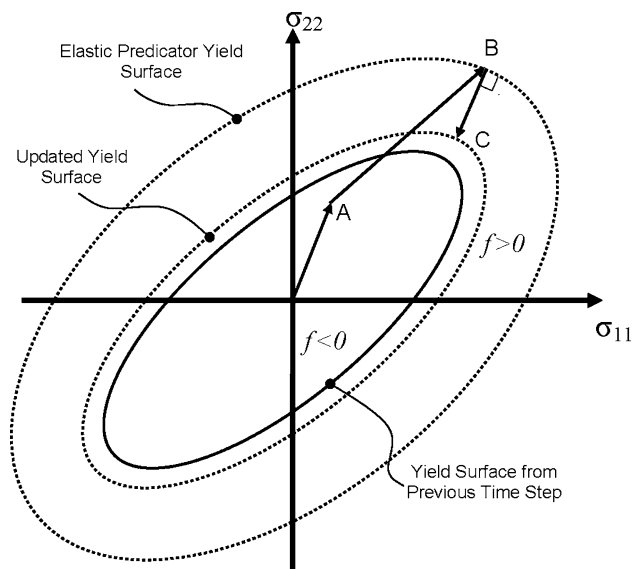
Table 4 Orthotropic quadratic yield-function coefficients for the 0°/90° cross-plied oriented UHMWPE fiber-based armor-grade composite material

a_{11}	a_{22}	a_{33}	a_{12}	a_{13}	a_{23}	a_{44}	a_{55}	a_{66}	R, GPa^2
8.2	1.0	1.0	6.0	6.0	6.3	0.3	0.3	0.4	3/97

Fig. 5 A schematic of the orthotropic yield surface and the normality flow rule

31, and 12 shear-failure modes (where indices used to designate the failure mode refer to the material principal directions/plane normals).

Within the present model, separate damage initiation/ continuation criteria are defined for the three principal-(ortho-tropic) material planes as:

$$g_{11,f}^2 = \left(\frac{\sigma_{11}}{\sigma_{11,f}(1-D_{11})}\right)^2 + \left(\frac{\sigma_{12}}{\sigma_{12,f}(1-D_{12})}\right)^2$$
$$+ \left(\frac{\sigma_{13}}{\sigma_{13,f}(1-D_{13})}\right)^2 \geq 1$$

$$g_{22,f}^2 = \left(\frac{\sigma_{22}}{\sigma_{22,f}(1-D_{22})}\right)^2 + \left(\frac{\sigma_{12}}{\sigma_{12,f}(1-D_{12})}\right)^2$$
$$+ \left(\frac{\sigma_{23}}{\sigma_{23,f}(1-D_{23})}\right)^2 \geq 1 \qquad \text{(Eq 11)}$$

$$g_{33,f}^2 = \left(\frac{\sigma_{33}}{\sigma_{33,f}(1-D_{33})}\right)^2 + \left(\frac{\sigma_{23}}{\sigma_{23,f}(1-D_{23})}\right)^2$$
$$+ \left(\frac{\sigma_{13}}{\sigma_{13,f}(1-D_{13})}\right)^2 \geq 1$$

where D defines the extent of material damage, subscripts $i, j = 1, 2, 3$ are used to denote the mode of damage whereas subscript f denotes the initial failure strength.

A normality flow rule based on the failure surface(s), analogous to that in the strength model, is used within the present failure model to define the components of the "crack-strain" increments.

Past the point of failure initiation, the relationship between the failure strength and the crack strain (i.e., the material constitutive law) is assumed to be linear. Consequently, a maximum "crack strain" e_{cr}^{max} is defined as a ratio $2G_f/\sigma_f L$, where L is the characteristic dimension of the computational cell undergoing fracture (Ref 20). In other words, a crack strain is introduced which defines the extent of material (damage induced) deformation past the point of failure initiation. The ratio e_{cr}/e_{cr}^{max} for a given mode of failure is generally denoted as the extent of material damage, D, and $D = 0$ at failure initiation and $D = 1.0$ at complete failure. An example of the relationship between the failure strength and the corresponding fracture energy, G_f, for a single mode of failure is shown schematically in Fig. 6.
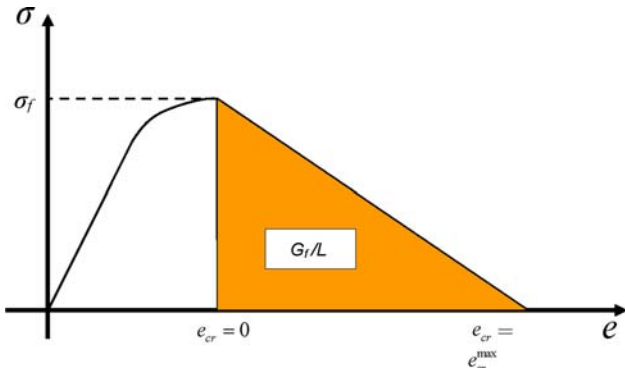
An Euler-backward procedure, analogous to that mentioned in the previous section, is used to update the stress state during an elastic/failure loading step. A schematic of this procedure for the failure surface associated with the first principal material plane is depicted in Fig. 7.

In summary, the orthotropic-softening damage model used in the present work includes parabolic stress-based damage initiation criteria (one criterion for each material principal plane), a normality flow rule, and a linear damage-induced softening constitutive relation for each failure strength. All the parameters for the orthotropic-softening damage model were determined using the previously mentioned finite element analyses pertaining to relatively simple mechanical tests of the armor-grade composite unit cell. A summary of the results obtained in this portion of the work is given in Table 5.

Erosion Model. The same erosion model was used as in the case of metallic materials present in the bullet, as discussed in section "Metallic Materials".

Fig. 7 A schematic of the orthotropic crack-softening surface, the normality flow rule, and the Euler-backward stress updating procedure

Table 5   Orthotropic damage-softening failure model parameters and erosion parameters for the 0°/90° cross-plied oriented UHMWPE fiber-based armor-grade composite material

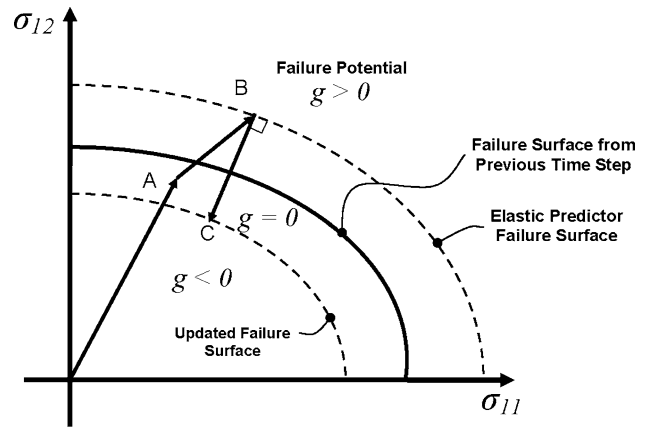| Parameter	Symbol	Unit	Value
Failure model			
Failure stress	σ_{11}	MPa	45.0
Failure stress	σ_{22}	MPa	245.0
Failure stress	σ_{33}	MPa	245.0
Failure stress	σ_{12}	MPa	15.0
Failure stress	σ_{23}	MPa	100.0
Failure stress	σ_{31}	MPa	15.0
Fracture energy	G_{11}	J/m^2	544.7
Fracture energy	G_{22}	J/m^2	30.0
Fracture energy	G_{33}	J/m^2	30.0
Fracture energy	G_{12}	J/m^2	1.46
Fracture energy	G_{23}	J/m^2	1.46
Fracture energy	G_{31}	J/m^2	1.46
Erosion model			
Erosion strain	ε	...	0.65

Fig. 6 A schematic of the stress-strain relationship accompanying a single-mode failure as considered within the present orthotropic crack-softening model

3. Results and Discussion

In this section, the material model for the 0°/90° cross-ply UHMWPE filament-based armor-grade composites developed in the present work is validated by comparing the computational results obtained in a series of transient nonlinear dynamics finite element analyses discussed in section "Problems Description, Modeling, and Simulations" with the experimental counterparts obtained in the work of Iremonger (Ref 33). Iremonger (Ref 33) investigated five armor panels (the constant panel-thickness ranged between 4.2 and 32 mm), used two types of bullets (M855 and M193, discussed earlier), and four initial bullet velocities (600, 700, 800, and 900 m/s). Thus, the full-factorial test matrix contains a total of $5 \times 2 \times 4 = 40$ experiments. However, not all 40 experiments were conducted in the work of Iremonger (Ref 33) and only selected results were reported for the experiments that were carried out. Specifically, three types of results were reported: (a) the success of composite-laminate target in stopping the bullet. Iremonger (Ref 33) used the following nomenclature: "*under matched*" (to denote the cases when the target-panel was successful in stopping the bullet), "*overmatched*" (to denote the cases when the panel was fully penetrated by the bullet but was able to absorb a substantial amount of the bullet's kinetic energy), and "*grossly overmatched*" (to denote the cases when the bullet was able to fully penetrate the panel by punching out a circular disk-shaped plug of the panel material without a significant loss in the bullets kinetic energy); (b) *postmortem* micrographs of the vertical cut sections of the target panel passing through the axis of the penetration hole; and (c) temporal-evolution plots for the target-panel back-face bulge height and the bulge diameter. In the remainder of this section, a comprehensive comparison will be given between the computational and the experimental results for each of these three sets of results.

3.1 The Success of Armor Test Panels in Stopping the Bullet

A comparison between the results pertaining to the success of different target panels in stopping the M855 bullet at different bullet velocities obtained experimentally by Iremonger (Ref 33) and their computational counterparts obtained in the present work is shown in Table 2. Clearly, overall agreement between the two sets of results is quite good suggesting that the present material model is capable of accounting for the essential features of the mechanical response of cross-plied UHMWPE filament-based armor-grade composites under ballistic loading conditions.

3.2 Spatial Distribution of the Mode and the Extent of Damage

Vertical-section micrographs of three perforated armor panels reported in Ref 33 are displayed in Fig. 8(a), 9(a), and 10(a). Due to copyright restrictions, only schematics of these micrographs are shown in these figures. The three micrographs correspond, respectively, to the following armor/bullet/test conditions. (a) 11 mm thick test panel/M855/600 m/s, Fig. 8(a); (b) 22 mm thick test panel/M855/800 m/s, Fig. 9(a); and (c) 22 mm thick test panel/M193/800 m/s, Fig. 10(a). The corresponding computational results revealing the spatial distribution of the mode and the extent of damage in the same armor panels obtained in the present work are displayed in Fig. 8(b), 9(b), and 10(b), respectively.
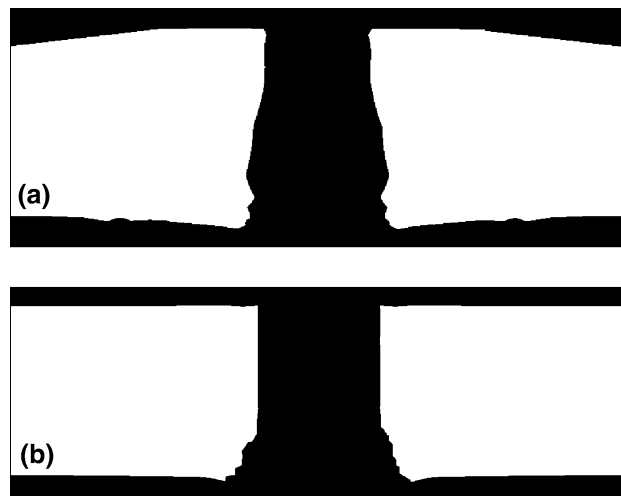

Fig. 8 A comparison between (as schematic of) the experimental results obtained in Ref 33, (a), and their computational counterparts obtained in the present work, (b), pertaining to the spatial distribution of damage in case of a M855 bullet initially propelled at a velocity of 600 m/s impacting an 11 mm thick test panel
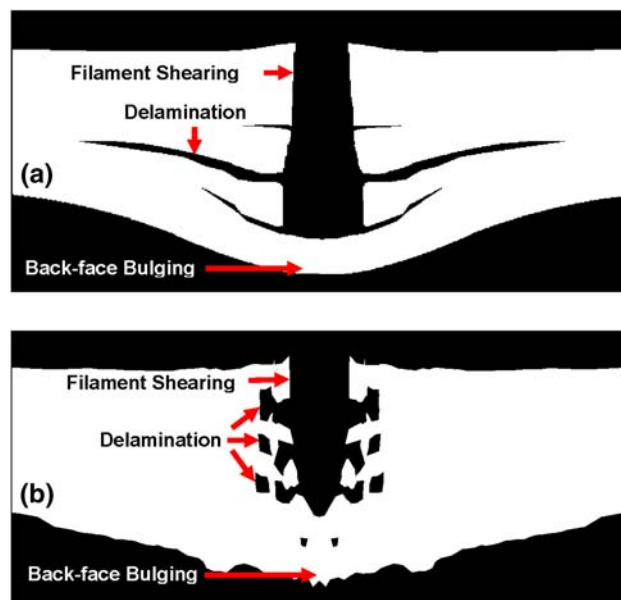

Fig. 9 A comparison between (as schematic of) the experimental results obtained in Ref 33, (a), and their computational counterparts obtained in the present work, (b), pertaining to the spatial distribution of damage in case of a M855 bullet initially propelled at a velocity of 800 m/s impacting an 22 mm thick test panel

A comparison between the results displayed in Fig. 8(a), 9(a), and 10(a) with the ones displayed in Fig. 8(b), 9(b), and Fig. 10(b), respectively, reveals that the overall agreement between the two sets of results is reasonable. More specifically: (a) Both the experiment, Fig. 8(a), and the computational analysis, Fig. 8(b), show a "*Punch-through*" mode of penetration (dominated by transverse shearing/cutting of the filaments and associated with relatively low absorption of the projectiles kinetic energy) in the case of 11 mm thick armor panel impacted by an M855 projectile at an initial velocity of
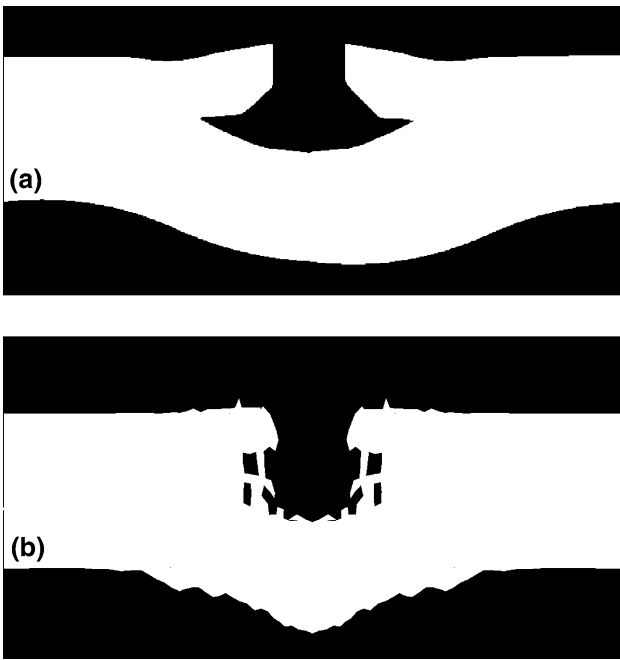
Fig. 10 A comparison between (as schematic of) the experimental results obtained in Ref 33, (a), and their computational counterparts obtained in the present work, (b), pertaining to the spatial distribution of damage in case of a M193 bullet initially propelled at a velocity of 800 m/s impacting an 22 mm thick test panel

600 m/s. In addition, the penetration-hole size and its variation through the armor-panel thickness are also reasonably well reproduced by the present material model, Fig. 8(a) versus (b); (b) Both the experiment and the computational analysis show only a partial penetration of the armor in the case of a 22 mm thick armor panel impacted by an M855 projectile at an initial velocity of 800 m/s, Fig. 9(a, b). The depth of the penetration hole is slightly underpredicted by the computational analysis. Further examination of Fig. 9(a, b) reveals that both the experiment and the computational analysis predict that initial penetration of the armor panel is first dominated by filament shearing/cutting and subsequently by filament/matrix debonding/delamination. It should be recalled that the present material model is based on homogenization of the constituent (filament and matrix) materials and, hence, defines an equivalent single-phase material. Consequently, delamination in the present computational analysis appears as a region of removed/eroded elements rather than a region where filament/matrix debonding has taken place. Despite these differences, the extent of delamination predicted by the current model appears comparable to that observed experimentally. Also, the extents of back-face bulging observed experimentally, Fig. 9(a), and the one predicted computationally, Fig. 9(b), are in reasonably good agreement; and (c) For the case of a 22 mm thick armor panel impacted by a non-armor-piercing M193 projectile at an initial velocity of 800 m/s, both the experiment, and the numerical results show only a partial penetration of the armor with comparable depth of the penetration holes, Fig. 10(a, b). As in the case of Fig. 9(a, b), the present computational analysis predicts reasonably well the extent of delamination within the armor and the extent of back-face bulging.

In the work of Iremonger (Ref 33), three distinct regimes of armor-panel failure were identified, when the panels were

subjected to armor-piercing and non-armor-piercing small-caliber projectiles: (a) an initial penetration phase dominated by shearing/cutting of the filaments by the projectile and, to a larger extent, by plastic deformation of the projectile; (b) an intermediate phase dominated by extensive filament/matrix delamination and destabilization and fragmentation of the projectile; and (c) the final phase dominated by extensive stretching of the filaments (responsible for high energy-absorption capacity of the armor-grade composites) and the resulting extensive bulging of the armor back-face. The computational results obtained in the present work (e.g., Fig. 9b) clearly confirmed the existence of these three phases of projectile/armor interaction suggesting that the proposed material model for the 0°/90° cross-plied UHMWPE-based armor-grade composites is physically sound.

3.3 Temporal Evolution of the Back-Face Bulge

In Ref 33, the temporal evolution of the armor back-face bulge height and diameter was reported only for the case of a 32 mm thick armor test panel, M855 bullet, and the initial bullet velocity of 900 m/s. The reported results for the bulge height and for the bulge diameter are displayed in Fig. 11(a) and (b), respectively, and they are denoted using filled circular symbols. The corresponding computational results obtained in the present work are also displayed in these figures and they are denoted using unfilled circular symbols. A simple examination of the results displayed in Fig. 11(a, b) reveals that: (a) while the initial rate of increase of the back-face bulge height predicted by the present analysis is comparable to that measured experimentally, Fig. 11(a), the computational results underpredict the bulge height by ∼10 mm. There are several potential reasons for this disagreement, the main one being: (i) both the initial projectile velocity and the bulge-height measurements utilized in the work of Iremonger (Ref 33) were associated with experimental errors as high as ±5% and (ii) the extents of projectile damage/fragmentation were likely different in the experiment and in the computational analysis. Unfortunately, no detail information was reported by Iremonger (Ref 33) regarding the extent of projectile damage/fragmentation. In other words, the observed experiment/computation discrepancy cannot be solely interpreted as a deficiency of the present model. The computed temporal evolution of the bulge-height displayed in Fig. 11(a) shows a decrease in the bulge-height after approximately 160 µs. This decrease is associated with the elastic relaxation of the armor-panel back-face after the projectile was defeated and pushed back. Similar observation was not made by Iremonger (Ref 33). Instead, the bulge height has continued to increase, Fig. 11(a). The reason for this discrepancy is that in the work of Iremonger (Ref 36) the projectile was typically left buried within the partially pene-trated armor panel preventing back-face elastic relaxation and (b) except for the very initial stage of armor penetration by the projectile, the experimentally measured and computationally predicted temporal evolutions of the back-face bulge diameter are in reasonably good agreement, Fig. 11(b).

3.4 A Brief Summary

The main objective of the present work was to develop, parameterize, and validate a simple physically based compu-tationally efficient material model for a prototypical 0°/90° cross-plied oriented polyethylene fiber-based armor-grade composite material. Parameterization of the newly developed
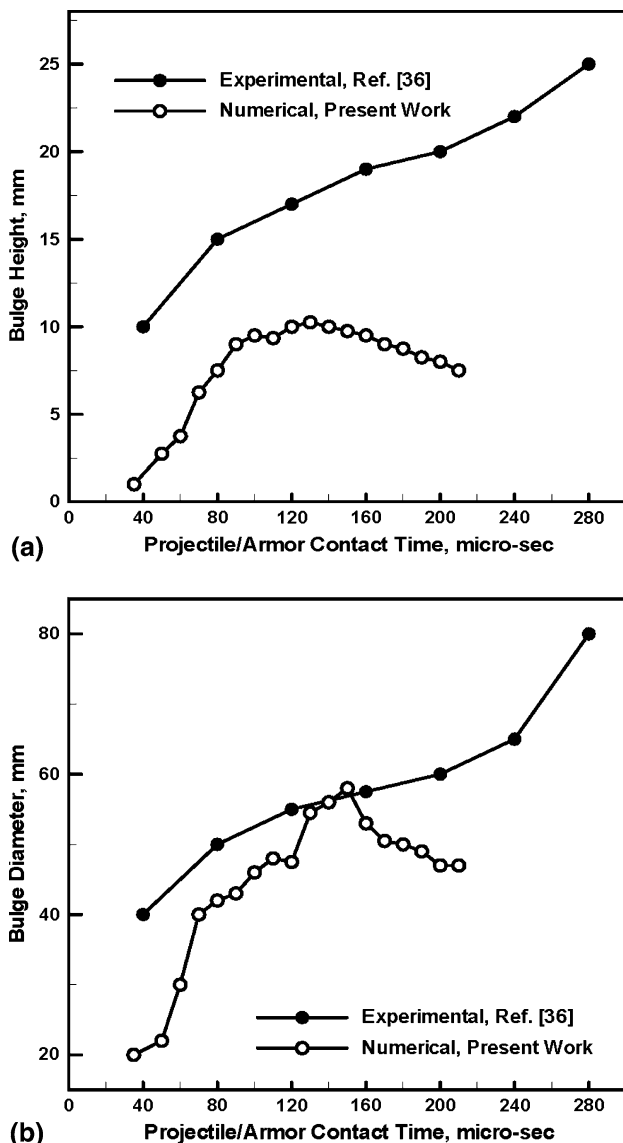
Fig. 11 A comparison between (as schematic of) the experimental results obtained in Ref 33 and their computational counterparts obtained in the present work, pertaining to the temporal evolution of: (a) the height and (b) the diameter of a delamination-induced bulge at the armor back-face for the case of a M855 bullet initially propelled at a velocity of 900 m/s impacting a 32 mm thick test panel

material model was carried out using the unit cell-based finite element analyses presented in our prior work (Ref 22). The material-model validation was carried out by constructing a transient nonlinear dynamics finite element model consistent with the experimental setup used in the experimental work of Iremonger (Ref 33). The key experimental results reported in Ref 33 were then compared with their computational counterparts to judge the validity of the present material model. The obtained level of qualitative and quantitative agreement between the two sets of results suggests that the proposed material model is capable of capturing the essential ballistic-resistance behavior of a prototypical 0°/90° cross-plied UHMWPE-based armor-grade composite material.

The present model is computationally about three times more efficient than the one developed in our previous work (Ref 22) while the results of the two models are quite comparable. The computational results based on the use of the material model reported in Ref 22 (not shown here for brevity) can be found in the same reference.

While the present work was focusing on the development, parameterization, and validation of the material model, in our future work, the model will be used to investigate in greater details the competition and interplay between various deformation, fracture, and energy-dissipation phenomena which control armors ability to defeat projectiles by absorbing their kinetic energy.

4. Conclusions

Based on the work presented and discussed in the present manuscript, the following main conclusions can be drawn:

1. A simple continuum damage-softening-based material model for the prototypical cross-plied unidirectional UHMWPE filament-based armor-grade composites developed and parameterized in the present work appears to be able to account for the key aspects of ballistic/mechanical response of these materials when impacted by armor-piercing and non-armor-piercing small-caliber bullets;
2. Specifically, the proposed material model can, for the most part, reasonably well account for the observed success of the armor panels of different areal densities in defeating the bullets at different initial bullet velocities, for the postmortem spatial distribution of damage within the panel, and for the temporal evolution of a bulge at the back face of the armor.
3. The transient nonlinear dynamics analyses based on the present material model clearly revealed three different phases of armor penetration by the projectile, the same phases observed experimentally (Ref 33), that is: (a) an initial filament shearing/cutting-dominated phase; (b) an intermediate phase characterized by pronounced filament/matrix debonding/decohesion; and (c) a final phase associated with extensive filament stretching armor-panel back-face bulging.

References

1. B.L. Lee, J.W. Song, and J.E. Ward, Failure of Spectra® Polyethylene Fiber-Reinforced Composites Under Ballistic Impact Loading, *J. Compos. Mater.*, 1994, **28**(13), p 1202–1226
2. B.L. Lee, T.F. Walsh, S.T. Won, H.M. Patts, J.W. Song, and A.H. Mayer, Penetration Failure Mechanisms of Armor-Grade Fiber Composites Under Impact, *J. Compos. Mater.*, 2001, **35**, p 1605–1635
3. J.G. Donovan, B. Kirkwood, and F. Figucia, "Development of Lower Cost Ballistic Protection," Technical Report Natick/TR-85/019L, U.S. Army Natick RD&E Center, Natick, MA, 1985
4. L.C. Lin, A. Bhatnagar, and H.W. Chang, Ballistic Energy Absorption of Composites, *Proceedings of the 22nd SAMPE International Technical Conference*, Nov 6-8, 1990 (Boston, MA), 1990, p 1–13

5. D.C. Prevorsek, Y.D. Kwon, and H.B. Chin, Analysis of the Temperature Rise in the Projectile and Extended Chain Polyethylene Fiber Composite Armor During Ballistic Impact and Penetration, *Polym. Eng. Sci.*, 1994, **34**, p 141–152

6. G. Zhu, W. Goldsmith, and C.K.H. Dharan, Penetration of Laminated Kevlar by Projectiles. I. Experimental Investigation, *Int. J. Solids Struct.*, 1992, **29**(4), p 399–420

7. G. Zhu, W. Goldsmith, and C.K.H. Dharan, Penetration of Laminated Kevlar by Projectiles. II. Analytical Model, *Int. J. Solids Struct.*, 1992, **29**(4), p 421–436

8. T.L. Schuman, S2000 Ballistic Hardened C3I Shelter, *Proceedings of the 24th SAMPE International Technical Conference*, Oct 20-22, 1992 (Toronto, Canada), 1992, p 280–290

9. C.L. Segal, High-Performance Organic Fibers, Fabrics and Composites for Soft and Hard Armor Applications, *Proceedings of the 23rd SAMPE International Technical Conference*, Oct 22-24, 1991 (New York), 1991, p 651–660

10. P.G. Riewald, F.H.H. FolgarYang, and W.F. Shaughnessy, Lightweight Helmet from a New Aramid Fiber, *Proceedings of the 23rd SAMPE International Tech. Conference*, Oct 22-24, 1991 (New York), 1991, p 684–695

11. T.S. Thomas, Facets of a Lightweight Armor System Design, *Proceedings of the 22nd SAMPE International Technical Conference*, Nov 6-8, 1990 (Boston, MA), 1990, p 304–318

12. D.C. Prevorsek and H.B. Chin, "Development of a LightWeight Spectra Helmet," Phase I Interim Technical Report from AlliedSignal Inc. to U.S. Army Natick RD&E Center, Natick, MA, DAAK60-87-C-0089/D, 1988

13. J.W. Song and G.T. Egglestone, Investigation of the PVB/PF Ratios on the Crosslinking and Ballistic Properties in Glass and Aramid Fiber Laminate Systems, *Proceedings of the 19th SAMPE International Technical Conference*, Oct 13-15, 1987, p 108–119

14. J.C. Smith, J.M. Blandford, and H.F. Schiefer, Stress-Strain Relationships in Yarns Subjected to Rapid Impact Loading: Part VI. Velocities of Strain Waves Resulting from Impact, *Text. Res. J.*, 1960, **30**(10), p 752

15. J.C. Smith, J.M. Blandford, and K.M. Towne, Stress-Strain Relationships in Yarns Subjected to Rapid Impact Loading: Part VIII. Shock Waves, Limiting Breaking Velocities, and Critical Velocities, *Text. Res. J*, 1962, **32**(1), p 67

16. D. Roylance, A. Wilde, and G. Tocci, Ballistic Impact of Textile Structures, *Text. Res. J*, 1973, **43**, p 34–41

17. P.M. Cunnif, An Analysis of the System Effects in Woven Fabric Under Ballistic Impact, *Text. Res. J.*, 1992, **62**(9), p 495–509

18. R.W. Dent and J.G. Donovan, "Projectile Impact with Flexible Armor—An Improved Model," Technical Report Natick/TR-86/044L, U.S. Army Natick RD&E Center, Natick, MA, 1986

19. C.Y. Hsieh, A. Mount, B.Z. Jang, and R.H. Zee, Response of Polymer Composites to High and Low Velocity Impact, *Proceedings of the 22nd SAMPE International Technical Conference*, Nov 6-8, 1990 (Boston, MA), 1990, p 14–27

20. N. Critescu, L.E. Malvern, and R.L. Sierakowski, Failure Mechanisms in Composite Plates Impacted by Blunt-Ended Penetrators, *Foreign Object Impact Damage to Composites*, ASTM STP #568, ASTM, Philadelphia, PA, 1975, p 159–172

21. D.S. Cairs and P.A. Lagace, Transient Response of Graphite/Epoxy and Kevlar/Epoxy Laminates Subjected to Impact, *AIAA J.*, 1989, **27**(11), p 1590–1596

22. M. Grujicic, G. Arakere, T. He, W.C. Bell, B. A. Cheeseman, C.-F. Yen, and B. Scott, A Ballistic Material Model for Cross-Plied Unidirectional Ultra-High Molecular-Weight Polyethylene Fiber-reinforced Armor-Grade Composites, *Mater. Sci. Eng, A*, 2008, **498**(1-2), p 231–241

23. R. Frissen, T. Peijs, and A. Verlinde, Modelling the Ballistic Impact Behaviour of High-performance Polyethylene Fiber Reinforced Laminates, *Proceedings of the 16th International Symposium on Ballistics*, Sept 2-28, 1996 (San Francisco, CA), 1996

24. P.M. Cunniff, Dimensionless Parameters for Optimization of Textile-Based Body Armor Systems, *Proceedings of the 18th International Symposium on Ballistics*, Nov 15-19, 1999 (San Antonio, TX), 1999, p 1303

25. R. Clegg, C. Hayhurst, J. Leahy, and M. Deutekom, Application of a Coupled Anisotropic Material Model to High Velocity Impact Response of Composite Textile Armour, *Proceedings of the 18th International Symposium on Ballistics*, Nov 15-19, 1999 (San Antonio, TX), 1999, p 791

26. A.M. Floyd, K. Williams, R. Varziri, K. Kanji, and A. Pourtasip, Through-Thickness Strain-Softening Damage Modelling of Composite Laminate, *Proceedings of the 18th International Symposium on Ballistics*, Nov 15-19, 1999 (San Antonio, TX), 1999, p 877

27. P.M. Cunniff and J. Ting, Development of a Numerical Model to Characterize the Ballistic Behavior of Fabrics, *Proceedings of the 18th International Symposium on Ballistics*, Nov 15-19, 1999 (San Antonio, TX), 1999, p 822

28. G.R. Johnson, R. Beissel, and P.M. Cunniff, A Computational Model for Fabrics Subjected to Ballistic Impact, *Proceedings 18th International Symposium on Ballistics*, Nov 15-19, 1999 (San Antonio, TX), 1999, p 962

29. X. Guan and N. Birnbaum, SPH Simulation of the Ballistic Perforation of GFRP, *Proceedings of the 18th International Symposium on Ballistics*, Nov 15-19, 1999 (San Antonio, TX), 1999, p 1107

30. M.J.N. Jacobs and J.L.J. Van Dingenen, Ballistic Protection Mechanisms in Personal Armour, *J. Mater. Sci.*, 2001, **36**, p 3137–3142

31. ANSYS/Autodyn version 11.0, User Documentation, Century Dynamics Inc., a subsidiary of ANSYS Inc., 2007

32. M. Grujicic, W.C. Bell, H. Marvi, I. Haque, B.A. Cheeseman, W.N. Roy, and R.R. Skaggs, A Computational Analysis of Survivability of a Pick-Up Truck Subjected to Mine Detonation Loads, *Multidiscip. Model. Mater. Struct.*, accepted for publication, June 2008

33. M.J. Iremonger, Polyethylene Composites for Protection against High Velocity Small Arms Bullets, *Proceedings of the 18th International Symposium on Ballistics*, Nov 15-19, 1999 (San Antonio, TX), 1999, p 946–953

34. M. Grujicic, B. Pandurangan, U. Zecevic, K.L. Koudela, and B.A. Cheeseman, Ballistic Performance of Alumina/S-2 Glass-Reinforced Polymer-Matrix Composite Hybrid Lightweight Armor Against Armor Piercing (AP) and Non-AP Projectiles, *Multidiscip. Model. Mater. Struct.*, 2007, **3**, p 287–312

35. B.A. Cheeseman and T.A. Bogetti, Ballistic Impact into Fabric and Compliant Composite Laminates, *Compos. Struct.*, 2003, **61**, p 161–173

36. ABAQUS – Version 6.7, User Documentation, Dassault Systems, 2007

37. M. Grujicic, Y.P. Sun, and K.L. Koudela, The Effect of Covalent Functionlization of Carbon Nanotube Reinforcements on the Atomic-Level Mechanical Properties of Poly-Vinyl-Ester-Epoxy, *Appl. Surf. Sci.*, 2007, **253**, p 3009–3021